

Negative refraction by a uniaxial wire medium with suppressed spatial dispersion

Mário G. Silveirinha*

Department of Electrical Engineering-Instituto de Telecomunicações, University of Coimbra, 3030 Coimbra, Portugal

Alexander B. Yakovlev†

Department of Electrical Engineering, University of Mississippi, University, Mississippi 38677, USA

(Received 2 April 2010; published 24 June 2010)

Here, we show that a structure formed by an array of metallic wires loaded with metallic patches may enable strong negative refraction even when the conductivity of the metal is very large, e.g., in the microwave regime. It is shown that the composite structure may be regarded as a uniaxial indefinite material loaded with impedance sheets, and that the negative refraction effect may be characterized using homogenization methods.

DOI: [10.1103/PhysRevB.81.233105](https://doi.org/10.1103/PhysRevB.81.233105)

PACS number(s): 42.70.Qs, 78.20.Ci, 41.20.Jb, 78.66.Sq

Negative refraction easily captures our imagination because the ray tracing contradicts our empirical understanding of the refraction effect. Even though such phenomenon is not observed in conventional dielectrics, it has been shown recently that several physical mechanisms permit its occurrence. The most well-known approach is based on materials with simultaneously negative permittivity and permeability, as suggested originally by V. Veselago.¹ There are, however, simpler and more robust routes to achieve negative refraction. For example, a conventional anisotropic material with optical axes tilted with respect to the interface may, for some directions of incidence, negatively refract the incoming wave (e.g., Ref. 2). Other interesting possibilities are based on photonic crystals^{3,4} and nonlocal materials.⁵ Another robust solution is based on indefinite anisotropic materials, such that the eigenvalues of the permittivity (or permeability) tensor have different signs.^{6,7} This negative refraction mechanism was recently demonstrated at optical frequencies using an array of metallic nanorods.^{8,9} However, such configuration is only effective in the optical domain where the plasmonic properties of metal play a dominant role. At lower infrared and microwave frequencies, due to the large conductivity of the metals, the array of nanorods is characterized by strong spatial dispersion, and consequently behaves very differently from a material with indefinite parameters.^{10–13}

Here, building on previous work,^{13–18} we confirm that despite these difficulties it is possible to tame the spatial dispersion effects in the metamaterial by attaching metallic patches to the wires—as originally suggested in Ref. 14—and that this modified configuration enables a strong broadband negative refraction effect. The configuration under study is depicted in Fig. 1. The metamaterial consists of an array of parallel metallic wires with radius r_w embedded in a dielectric with permittivity ϵ_h . The wires are loaded with square metallic patches, such that the spacing between the patches along the z direction is equal to h . The transverse lattice constant is a and the gap width is g . The geometry of the structure resembles in part the so-called mushroom high-impedance surface.¹⁹ A time variation of the form $\exp(-i\omega t)$ is assumed and suppressed. Here, we model the structured metal-dielectric slab as a continuous local uniaxial medium described by the permittivity tensor,

$$\frac{\bar{\bar{\epsilon}}}{\epsilon_0} = \epsilon_h(\hat{\mathbf{u}}_x\hat{\mathbf{u}}_x + \hat{\mathbf{u}}_y\hat{\mathbf{u}}_y) + \epsilon_{zz}\hat{\mathbf{u}}_z\hat{\mathbf{u}}_z, \quad (1)$$

loaded at the planes $z=0, -h, -2h, \dots, -L$ that contain the metallic patches with a sheet admittance^{15,16}

$$Y_g = -i\frac{1}{\eta_0}\epsilon_{qs}\frac{2a}{\pi}\frac{\omega}{c}\ln\left[\csc\left(\frac{\pi g}{2a}\right)\right], \quad (2)$$

where \csc is the co-secant function, and η_0 and c are the impedance and speed of light in vacuum, respectively. In the above, $\epsilon_{qs}=\epsilon_h$ for planes of patches that are interior to the structure, and $\epsilon_{qs}=(\epsilon_h+1)/2$ for the planes of patches located at the upper and lower interfaces ($z=0$ and $z=-L$). The permittivity along z is $\epsilon_{zz}=\epsilon_h-\beta_p^2c^2/\omega^2$, where $\beta_p=[2\pi/(\ln(a/2\pi r_w)+0.5275)]^{1/2}/a$ is the plasma wave number.

It is also possible to describe the combined response of the metallic wires and patches in terms of a continuous material model,^{13,14} but the results of a detailed analysis (not reported here) show that such approximation tends to be significantly less accurate, particularly near the plasma frequency of the wire medium. The permittivity model (1) is obtained from the nonlocal dielectric function $\bar{\bar{\epsilon}}(\omega, \mathbf{k})$ of the wire medium,¹⁰ by setting the wave vector \mathbf{k} equal to zero. This can be justified by noting that the role of the patches is to ensure that current along the wires is practically constant within the regions delimited by two adjacent planes of patches.^{15,16} Hence, the electromagnetic fields are essentially independent of z within such regions, $d/dz \approx 0$, and thus, the effective response of the wires when attached to the patches is coincident with that of a wire medium with no patches for the case where the currents along the wires are independent of z .^{15,16} This yields the *local* effective permittivity Eq. (1) because the condition $d/dz \approx 0$ is equivalent to $k_z \approx 0$ in the spectral domain.

In order to validate the homogenization model, we consider a scattering problem where a transverse magnetic (TM) plane wave with magnetic field $\mathbf{H}=\mathbf{H}_0^{inc}e^{i\mathbf{k}^{inc}\cdot\mathbf{r}}\hat{\mathbf{u}}_x$ and incident wave vector $\mathbf{k}^{inc}=(\omega/c)(\sin\theta_i\hat{\mathbf{u}}_y-\cos\theta_i\hat{\mathbf{u}}_z)$ illuminates a structured material slab characterized by the following normalized parameters: $g=0.1a$, $h=a$, $r_w=0.025a$, $\epsilon_h=10.2$, and $L=4h$ (the slab is formed by $N_{pl}=5$ planes of metallic

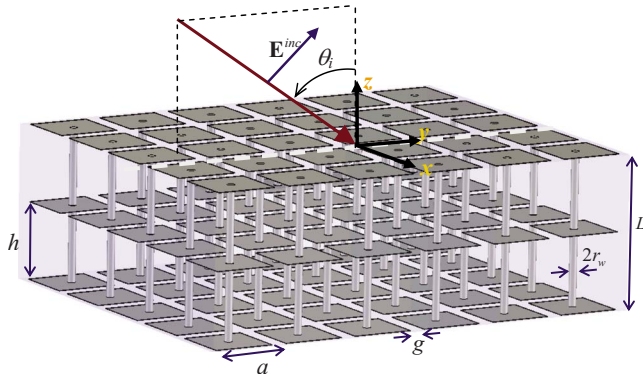


FIG. 1. (Color online) Geometry of a metamaterial slab formed by metallic wires attached to metallic patches.

patches). The transmission and reflection coefficients under plane-wave incidence are calculated as usual by writing the fields in the regions delimited by the sheet admittances in terms of plane waves—determined from the permittivity function Eq. (1)—and by imposing suitable boundary conditions at the interfaces ($z=0, -h, \dots, -L$). Specifically, at a generic interface $z=z_0$ the tangential component of the electric field is continuous $E_y|_{z_0^+}=E_y|_{z_0^-}$, whereas the tangential magnetic field verifies the sheet impedance boundary condition: $H_x|_{z_0^+}-H_x|_{z_0^-}=Y_g E_y|_{z_0}$, with Y_g given by Eq. (2).^{15,16} The homogenization results for the amplitude and phase of the transmission coefficient T and incidence along $\theta_i=30^\circ$ are depicted in Fig. 2(a) (dashed lines). These curves compare very well with full-wave results obtained with CST Micro-

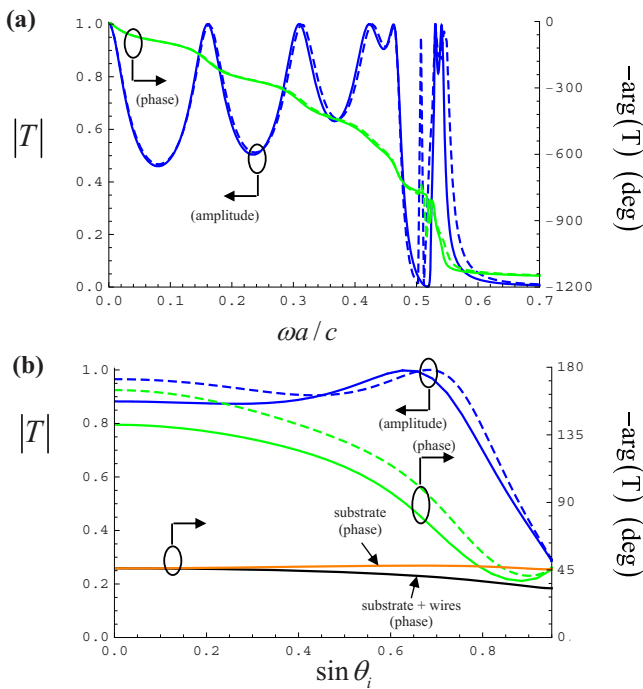


FIG. 2. (Color online) Amplitude and phase of the transmission coefficient under plane-wave incidence. Solid lines: full-wave results (Ref. 20); Dashed lines: analytical model. (a) Variation with the normalized frequency for $\theta_i=30^\circ$. (b) Variation with (the sine of) the angle of incidence at $\omega a/c=0.45$.

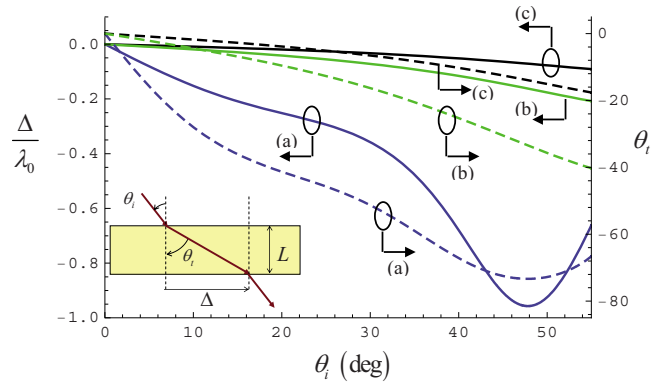


FIG. 3. (Color online) Spatial shift Δ (solid lines) and angle of transmission θ_t (dashed lines) as a function of the angle of incidence. (a) $\omega a/c=0.45$, (b) $\omega a/c=0.39$, (c) wire medium with no patches at $\omega a/c=0.45$.

wave Studio²⁰ [solid lines in Fig. 2(a)], except for some discrepancies near to the plasma resonance $\omega_p=c\beta_p/\sqrt{\epsilon_h}$ which occurs at the normalized frequency $\omega a/c=0.51$ ($\epsilon_{zz}=0$). In Fig. 2(b), the amplitude and phase of T are shown as a function of the angle of incidence (blue and green curves, respectively) at the normalized frequency $\omega a/c=0.45$ ($\epsilon_{zz}=-2.9$), showing a fairly good agreement with the full-wave simulations (for frequencies farther from the plasma resonance the agreement is greatly improved).

Since the results of Fig. 2 support that in the presence of the patches the wire medium behaves as a uniaxial indefinite material with no spatial dispersion, consistent with the findings of Refs. 13–16, it is interesting to investigate if the structured slab may as well enable negative refraction. Following Ref. 5, a simple and convenient way of studying this is to look at the variation of the phase of $T(\omega, k_y)=|T|e^{-i\phi}$ with θ_i . Specifically, it was proven in Ref. 5 that the spatial shift Δ (see the inset of Fig. 3) suffered by a quasi-plane-wave beam that illuminates an arbitrary metamaterial slab is given by $\Delta \approx d\phi/dk_y$, where $k_y=\omega/c \sin \theta_i$ is the transverse wave number of the incident wave and $\phi=-\arg T$. The formula is more accurate for thick slabs and assumes that the amplitude of the transmission coefficient varies slowly with small variations of the angle of incidence (which typically is not the case for wide incident angles). Thus, negative refraction occurs when $\Delta < 0$, that is if the phase of the transmission coefficient decreases with k_y (i.e., with the angle of incidence θ_i).⁵

One can see in Fig. 2(b) that at the normalized frequency $\omega a/c=0.45$ the angle $\phi=-\arg T$ decreases steadily with the angle of incidence (green curves), except for grazing incidence where the formula $\Delta \approx d\phi/dk_y$ is not applicable as mentioned previously. This confirms our intuition that the suppression of spatial dispersion in the wire medium favors the emergence of negative refraction. It is interesting to note the contrast between the behavior of ϕ in the presence of the patches [green curves in Fig. 2(b)] with its variation when the patches are removed and the structured material consists solely of vertical wires embedded in the dielectric substrate (black curve). Indeed, in the latter case, due to the effects of spatial dispersion in the wire medium, the slope of the phase

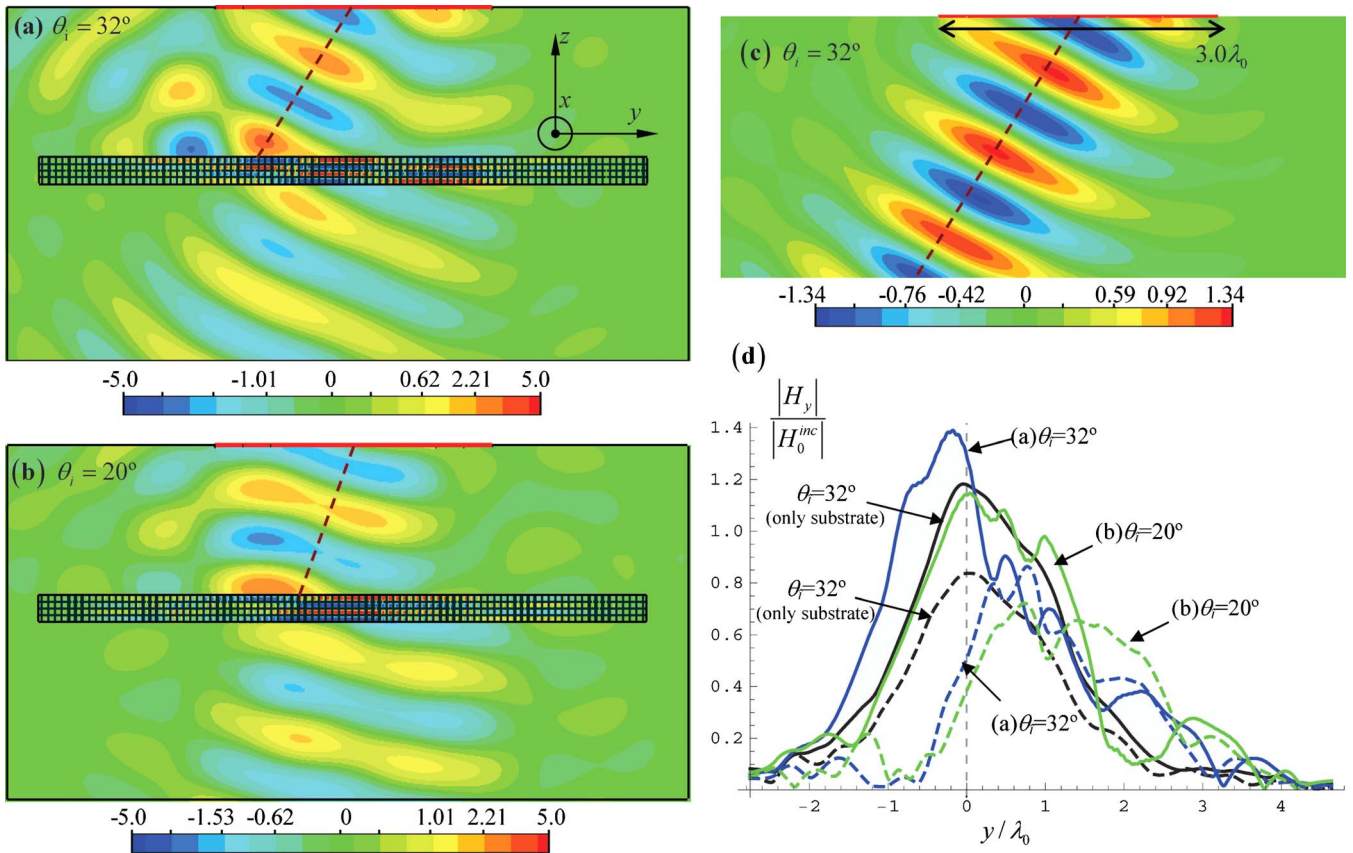


FIG. 4. (Color online) A Gaussian beam with HPBW $\approx 1.6\lambda_0$ illuminates a finite width metamaterial slab ($W_y=90a$) periodically extended along the x direction. The figure shows snapshots of the magnetic field, $H_y(t=0)$, for (a) $\omega a/c=0.45$ and $\theta_i=32^\circ$, (b) $\omega a/c=0.46$, and $\theta_i=20^\circ$, (c) incident beam for $\theta_i=32^\circ$ (with no slab). (d) Magnetic field profile normalized to the intensity of the incoming beam at the input interface (solid lines) and at the output interface (dashed lines) for the cases (a) and (b) and also when all the metallic implants are absent.

characteristic is quite small (even though it remains negative), and consequently the corresponding spatial shift is near to zero. This is consistent with the findings of Ref. 2 where it was shown that an array of parallel wires transports the incoming beam from the input interface to the output interface through a parallel projection. In Fig. 2(b), the orange line represents the phase characteristic of the slab ($\epsilon_h=10.2$) when the wires and patches are removed. As expected, now ϕ increases slightly with the angle of incidence (except for grazing incidence), consistent with the fact that in a regular dielectric a quasiplane wave is positively refracted.

In order to further characterize the negative refraction effect, we have calculated explicitly the spatial shift Δ and the angle of transmission θ_t (see the inset of Fig. 3) as a function of θ_i . The angle of transmission may be estimated using the formula $\theta_t = \tan^{-1} \Delta/L$.⁵ The results are shown in Fig. 3 and have been obtained using the analytical model based on homogenization theory. It can be seen (curves *a*) that for $\omega a/c=0.45$ the negative refraction is quite strong and that θ_t is typically larger, in absolute value, than θ_i . For $\theta_i=48^\circ$ the spatial phase shift may be comparable to one wavelength, even if the thickness of the slab is only $L=0.29\lambda_0$. The negative refraction effect is broadband and is observed for frequencies below the plasma resonance. For example, curves (b) in Fig. 3 represent Δ and θ_t for the normalized frequency

$\omega a/c=0.39$. It is evident that the negative refraction strength for this case is still quite meaningful, even though it is already much weaker than in the case $\omega a/c=0.45$. In fact, the negative refraction becomes progressively weaker away from the plasma resonance. Above the plasma resonance $\epsilon_{zz}>0$ and the wave is positively refracted. When the metallic patches are removed from the system—keeping the metallic wires embedded in the dielectric—(curves *c*) any possible negative refraction effects are as well very much weakened. This is evident from a comparison between curves (c) and (a) in Fig. 3.

In order to confirm these findings based on homogenization theory, we have simulated the electromagnetic response of a metamaterial slab illuminated by a Gaussian beam using CST Microwave Studio.²⁰ The considered Gaussian beam has a field distribution independent of the x coordinate. The geometrical parameters of the metamaterial are kept the same as in the previous examples, except that the width of the structure along the y direction is now finite and equal to $W_y=90a$. For simplicity, the structure is assumed periodic along the x direction (period is equal to a). The effect of realistic loss is considered in the simulation: the metallic components are assumed to be made of copper ($\sigma=5.8 \times 10^7$ S/m) and the loss tangent of the dielectric is $\tan \delta = 0.0015$ (dielectric substrates with similar properties are

commercially available, e.g., RT/DUROID 6010LM). The Gaussian beam is created in CST Microwave Studio by the simultaneous excitation of 10 adjacent waveguide ports. Each port has the electrical width $0.3\lambda_0$ at the design frequency. The amplitude and phase of each waveguide port are chosen so that the wave radiated by the port array mimics the profile of a Gaussian beam and propagates along a desired direction θ_i in the yo z plane. A snapshot of the magnetic field associated with the Gaussian beam at the frequency $\omega a/c = 0.45$ and for $\theta_i = 32^\circ$ is depicted in Fig. 4(c) (in the absence of the metamaterial slab). The half-power beamwidth (HPBW) at the front interface of the metamaterial slab is approximately $1.6\lambda_0$. The red line in the top of Fig. 4(c) indicates the location of the port array. In all the simulations the lattice constant was taken equal to $a = 22$ mm.

A small sample of the results that we obtained with CST Microwave Studio is depicted in Fig. 4. In panel (a) we depict a snapshot ($t=0$) of the magnetic field for the frequency of operation $\omega a/c = 0.45$ and for the angle of incidence $\theta_i = 32^\circ$ (see also Ref. 21). It is clearly seen that the transmitted beam suffers a significant negative lateral spatial shift, demonstrating the emergence of very strong negative refraction. Similar results are depicted in panel (b) of the same figure, now for $\omega a/c = 0.46$ and $\theta_i = 20^\circ$. The magnetic field profiles at the upper (solid lines) and lower (dashed lines) interfaces of the metamaterial slab are depicted in panel (d) of Fig. 4. They plainly show that the Gaussian beam is strongly refracted by the structured slab and that the spatial shift suffered by the beam is a significant fraction of the wavelength. The theoretical values (based on the analytical model) for the

spatial shift in the cases associated with panels (a) and (b) are, respectively, $\Delta = -0.40\lambda_0$ and $\Delta = -0.33\lambda_0$, which are reasonably consistent with (but may underestimate) the values that can be inferred from Fig. 4. Nevertheless, it should be mentioned that due to computational limitations our Gaussian beam cannot be exactly regarded as a quasiplane wave since its HPBW is only marginally larger than $1.5\lambda_0$, and thus the results of the analytical model should be regarded as rough qualitative estimations. As a control numerical test, we also show in Fig. 4(d) the profiles of the magnetic field when both the patches and metallic wires are absent and the slab is a dielectric with permittivity $\epsilon_h = 10.2$. As expected, given the relatively high value of ϵ_h , in such circumstances the spatial shift is nearly zero (similar results are obtained in the presence of wires without patches). It is also clear from the results of Fig. 4 that due to the effect of loss and reflections the level of the transmitted beam is somewhat weaker than that of the incident beam, even though the global level of transmission is clearly quite satisfactory.

In conclusion, we have confirmed that by attaching metallic patches to a wire array it is possible to suppress the spatial dispersion effects, and that this enables very strong negative refraction near the plasma resonance of the wire medium. This extends to lower frequencies the results of Refs. 8 and 9, which only apply when the plasmonic response of the metal is dominant (optical regime). This metamaterial may be used to design a planar lens that provides partial focusing.⁷

*mario.silveirinha@co.it.pt

†yakovlev@olemiss.edu

¹V. Veselago, *Sov. Phys. Usp.* **10**, 509 (1968).

²T. Morgado and M. G. Silveirinha, *New J. Phys.* **11**, 083023 (2009).

³M. Notomi, *Phys. Rev. B* **62**, 10696 (2000).

⁴E. Cubukcu, K. Aydin, E. Ozbay, S. Foteinopoulou, and C. M. Soukoulis, *Nature (London)* **423**, 604 (2003).

⁵M. G. Silveirinha, *Phys. Rev. B* **79**, 153109 (2009).

⁶D. R. Smith and D. Schurig, *Phys. Rev. Lett.* **90**, 077405 (2003).

⁷D. R. Smith, D. Schurig, J. J. Mock, P. Kolinko, and P. Rye, *Appl. Phys. Lett.* **84**, 2244 (2004).

⁸J. Yao, Z. Liu, Y. Liu, Y. Wang, C. Sun, G. Bartal, A. M. Stacy, and X. Zhang, *Science* **321**, 930 (2008).

⁹Y. Liu, G. Bartal, and X. Zhang, *Opt. Express* **16**, 15439 (2008).

¹⁰P. A. Belov, R. Marques, S. I. Maslovski, I. S. Nefedov, M. Silveirinha, C. R. Simovski, and S. A. Tretyakov, *Phys. Rev. B* **67**, 113103 (2003).

¹¹M. G. Silveirinha, *Phys. Rev. E* **73**, 046612 (2006).

¹²M. G. Silveirinha, P. A. Belov, and C. R. Simovski, *Phys. Rev. B* **75**, 035108 (2007).

¹³S. I. Maslovski and M. G. Silveirinha, *Phys. Rev. B* **80**, 245101 (2009).

¹⁴A. Demetriadou and J. B. Pendry, *J. Phys.: Condens. Matter* **20**, 295222 (2008).

¹⁵O. Luukkonen, M. G. Silveirinha, A. B. Yakovlev, C. R. Simovski, I. S. Nefedov, and S. A. Tretyakov, *IEEE Trans. Microwave Theory Tech.* **57**, 2692 (2009).

¹⁶A. B. Yakovlev, M. G. Silveirinha, O. Luukkonen, C. R. Simovski, I. S. Nefedov, and S. A. Tretyakov, *IEEE Trans. Microwave Theory Tech.* **57**, 2700 (2009).

¹⁷O. Luukkonen, P. Alitalo, F. Costa, C. Simovski, A. Monorchio, and S. Tretyakov, *Appl. Phys. Lett.* **96**, 081501 (2010).

¹⁸M. J. Lockyear, A. P. Hibbins, and J. R. Sambles, *Phys. Rev. Lett.* **102**, 073901 (2009).

¹⁹D. Sievenpiper, L. Zhang, R. Broas, N. Alexopolous, and E. Yablonovitch, *IEEE Trans. Microwave Theory Tech.* **47**, 2059 (1999).

²⁰CST Microwave Studio 2009, CST GmbH, <http://www.cst.com>

²¹See supplementary material at <http://link.aps.org/supplemental/10.1103/PhysRevB.81.233105> for the time animation of Fig. 4(a).